

The VVDS-VLA Deep Field:

III. GMRT observations at 610 MHz and the radio spectral index properties of the sub-mJy population*

M. Bondi¹, P. Ciliegi², T. Venturi¹, D. Dallacasa^{3,1}, S. Bardelli², E. Zucca², R.M. Athreya⁴, L. Gregorini^{5,1}, A. Zanichelli¹, O. Le Fèvre⁶, T. Contini⁷, B. Garilli⁸, A. Iovino⁹, S. Temporin⁹, and D. Vergani⁸

¹ INAF - Istituto di Radioastronomia, Via Gobetti 101, I-40129 Bologna, Italy

² INAF - Osservatorio Astronomico di Bologna, Via Ranzani 1, I-40127, Bologna, Italy

³ Università degli Studi di Bologna, Dipartimento di Astronomia, Via Ranzani 1, I-40127 Bologna, Italy

⁴ NCRA, Tata Institute of Fundamental Research Pune University Campus, Post Bag 3, Ganeshkhind Pune 411007, India

⁵ Università degli Studi di Bologna, Dipartimento di Fisica, Via Irnerio 46, I-40126 Bologna, Italy

⁶ Laboratoire d'Astrophysique de Marseille, UMR 6110 CNRS-Université de Provence, BP8, 13376 Marseille Cedex 12, France

⁷ Laboratoire d'Astrophysique de l'Observatoire Midi-Pyrénées (UMR 5572) - 14, avenue E. Belin, F31400 Toulouse, France

⁸ IASF-INAF - via Bassini 15, I-20133, Milano, Italy

⁹ INAF-Osservatorio Astronomico di Brera - Via Brera 28, Milan, Italy

Received 22 September 2006 / Accepted 17 October 2006

ABSTRACT

Aims. We present the low frequency (610 MHz) radio source counts of the VVDS-VLA field and investigate the radio spectral index properties of the sub-mJy population.

Methods. We use new deep (r.m.s. $\simeq 50 \mu\text{Jy}/\text{beam}$) observations of the VVDS-VLA field obtained at 610 MHz with the GMRT and matched in resolution (6 arcsec) with already available VLA data at 1.4 GHz on the same field.

Results. We find evidence of a change of the dominant population of radio sources below 0.5 mJy (at 1.4 GHz): between 0.15 and 0.5 mJy the median spectral index is significantly flatter ($\alpha = -0.46 \pm 0.03$) than that of brighter sources ($\alpha = -0.67 \pm 0.05$). A relevant contribution below 0.5 mJy from a population of flat spectrum low luminosity compact AGNs and radio quiet QSOs could explain this effect. At even fainter flux density, between 0.10 and 0.15 mJy at 1.4 GHz, the median spectral index steepens again ($\alpha = -0.61 \pm 0.04$) suggesting that the contribution of starburst galaxies becomes important below ~ 0.2 mJy. Finally we present a sample of 58 candidate ultra-steep sources with radio flux density from one to two orders of magnitude lower than any other sample of such objects.

Key words. Surveys – Radio continuum: galaxies – Methods: data analysis

1. Introduction

The "normal" population of radio sources with flux densities greater than a few mJy is fully explained in terms of radio loud active galactic nuclei (AGN) hosted by elliptical galaxies. At fainter flux densities, now extending to μJy levels, the radio source counts are increasingly dominated by contributions from other populations, such as radio-quiet AGNs mainly hosted by elliptical galaxies and starbursts in late-type galaxies, whose radio emission is the result of massive star formation and associated supernovae activity (Windhorst et al. 1985; Benn et al. 1993; Norris et al. 2005; Hammer et al. 1995; Richards et al. 1998; Afonso et al. 2005; Prandoni et al. 2001; Georgakakis et al. 1999; Gruppioni et al. 1999).

Far-infrared and X-ray observations have also provided further support for both starburst and AGN processes in the sub-mJy radio sources

(Afonso et al. 2001, 2006; Georgakakis et al. 2003, 2004). In the radio domain, the properties of the faint radio population have been mainly obtained from samples selected at 1.4 GHz (e.g., Richards 2000; Ciliegi et al. 1999; Bondi et al. 2003; Hopkins et al. 2003; Morganti et al. 2004; Huynh et al. 2005). Subsequent follow-up observations, carried out at higher frequencies (5 GHz or 8.4 GHz; e.g., Donnelly et al. 1987; Ciliegi et al. 2003; Fomalont et al. 2006) have been used to infer the triggering mechanism of the radio emission. In fact, the radio/optical morphology (compact or extended) and the radio spectrum (flat or steep) can help discriminate between emission from starbursts and/or AGNs and understanding the interaction between them. However, the angular size of the radio emission can be a definite discriminator only at very high resolution (< 0.05 arcsec, Garrett et al. 2001; Garrett et al. 2005), while the radio spectral properties, despite the extensive work done in recent years, can be interpreted in different ways and suffer from small number statistics.

* Table 1 is only available in electronic form at the CDS via <http://cdsweb.u-strasbg.fr/cgi-bin/qcat?J/A+A>

Analyzing rather small samples ($\lesssim 60$ sources) of sub-mJy sources, several authors (Donnelly et al. 1987; Gruppioni et al. 1997; Ciliegi et al. 2003) have found that the fraction of flat spectrum objects increases going to fainter density flux. Recently, with a more robust statistical significance, Prandoni et al. (2006) confirmed this result for a sample of 131 radio sources extracted from the ATESP survey. However, it is not yet established at which flux density level the flattening of the spectral index occurs.

At μJy level, Windhorst et al. (1993) found a median spectral index of -0.35 ($S \propto \nu^\alpha$), which, combined with the rather large linear size of the radio sources, has suggested synchrotron emission in distant galactic disks for the extended steep-spectrum sources and thermal Bremsstrahlung from large-scale star formation for the extended flat-spectrum sources. Recently, from the analysis of a sample of 47 radio sources, Fomalont et al. (2006) found that the spectral index may steepen for sources fainter than $75 \mu\text{Jy}$ and that in at most 40% of the μJy population the radio emission is associated with AGN emission, while the rest is mostly a consequence of star formation.

In this context the radio data of the VVDS-VLA Deep survey at 1.4 GHz (Bondi et al. 2003, Paper I) are perfectly suited for the study the properties of the sub-mJy population. From the deep radio observations carried out with the VLA, a catalogue containing 1054 radio sources detected down to a 5σ limit of $\simeq 80 \mu\text{Jy}$ was extracted. About 74% of the whole sample was optically identified using UBVRI and K data at an equivalent limiting magnitude of $V_{AB} = 26.2$ (Ciliegi et al. 2005, Paper II). The color and photometric redshift analysis of the optical counterparts show that radio detection preferentially selects galaxies with higher intrinsic optical luminosity and that most of the faintest radio sources are likely to be associated with relatively low radio luminosity objects at relatively modest redshift, rather than radio-powerful, AGN type objects at high redshift. The authors found that the majority of radio sources below 0.15 mJy are indeed late-type star-forming galaxies and that the radio sources without an optical counterpart probably contain a significant fraction of obscured and/or high redshift galaxies.

In this paper we present GMRT radio observations at 610 MHz of the VVDS-VLA field (Sect. 2). We discuss the methods used to derive the 5σ catalogue of 514 radio sources (Sect. 3) and present the radio source counts at 610 MHz down to 0.3 mJy (Sect. 4). Furthermore, using the 1.4 GHz catalogue obtained in Paper I, we investigate the radio spectral index properties of the sub-mJy radio sources and the relationships between the radio spectral index and the optical properties (Sect. 5). Finally we introduce a small sample of faint candidate ultra-steep spectrum radio sources (Sect. 6).

2. GMRT observations & data reduction

2.1. Observations

The VVDS-VLA field (RA(J2000) = 02:26:00 DEC(J2000) = $-04:30:00$, hereafter F02 field) was observed at the radio frequency of 610 MHz with the Giant Meter-Wave Radio Telescope (GMRT) in August 2004 for a total time of 24 hours (plus a short backup observation of about 4 hours in December 2004 to recover time lost during the run). At 610 MHz the GMRT has an angular resolution of about 6 arcsec

and a primary beam of 43 arcmin (FWHM). To observe the whole field with a sensitivity as uniform as possible, the 1 sq. deg. area of F02 was covered with a grid of 5 pointings: one in the field center and the other four displaced by 15 arcmin in both right ascension and declination from the central pointing. Each pointing was observed for about 5.5 hours.

Both the lower and upper sidebands, centered around 610 MHz, were recorded yielding to a total bandwidth of 32 MHz. The observations were carried out using 128 channels in each band and a spectral resolution of 125 kHz. In this way it was also possible to reduce the effects of narrow-band interferences since only the channels affected by the interferences, instead of the whole bandwidth, can be removed from the data. The radio sources 3C48 and 3C147 were observed at the beginning and at the end of the run as primary flux density and bandpass calibrators. The nearby source J0241-082 was observed every 30 minutes to provide secondary amplitude and phase calibration.

2.2. Data reduction

The data were reduced and analyzed using the package AIPS developed by the National Radio Astronomy Observatory. The amplitude and bandpass calibration were derived from daily observations of 3C 48 and 3C 147 assuming a flux density of 29.43 Jy and 38.26 Jy, respectively. After the bandpass calibration the central channels of each sideband were averaged to 6 channels of 1.75 MHz each, producing a total effective bandwidth of 21 MHz. The AIPS tasks UVLIN and CLIP were used to flag bad visibility data resulting from residual radio frequency interferences, receiver problems or correlator failures.

For each of the five pointings we imaged a field of about 51×51 arcmin (2048×2048 pixels with a pixel size of 1.5 arcsec), roughly the area of the whole primary beam, along with a number of smaller images centered on off-axis sources that can produce confusing grating rings in the imaged area. To avoid distortions due to the use of two-dimensional FFT to approximate the curved celestial sphere, the 2048×2048 pixels area of each pointing was not deconvolved as a single image, but was split into four 1024×1024 sub-images (e.g., Perley 1999).

At the end of the self-calibration deconvolution iteration scheme, the sub-images of all the 5 fields were combined together using the AIPS task FLATN and corrected for the primary beam response of GMRT at 610 MHz to produce the final mosaic with a resolution of 6 arcsec. The average noise over the whole 1 square degree field in the mosaic map is about $50 \mu\text{Jy}/\text{beam}$ providing a dynamic range greater than 2000, consistent with that expected. In Fig. 1 we show the final image of the 1 square degree field in units of signal-to-noise ratio.

3. The 610 MHz radio source catalogue

3.1. The noise map

To select a sample of sources above a given threshold, defined in terms of local signal-to-noise ratio, we derived the noise image following the same procedure adopted for the 1.4 GHz observations and using the software package SExtractor (Bertin & Arnouts 1996). SExtractor computes an estimator for the local background in each mesh of a grid

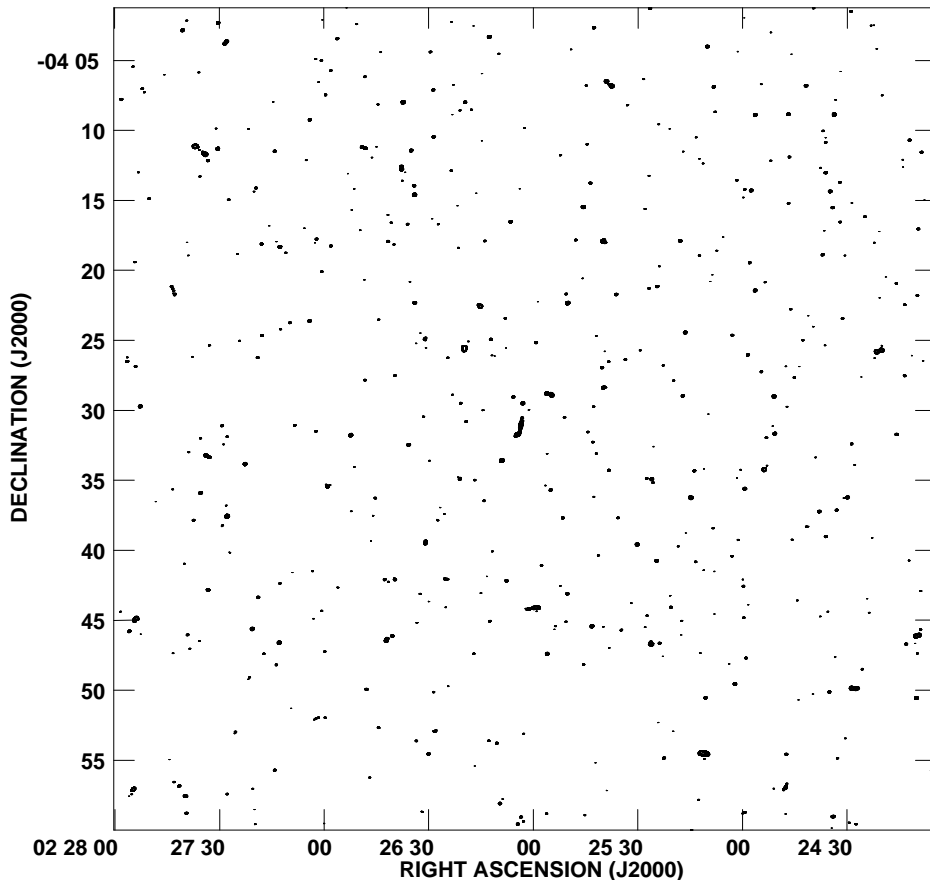


Fig. 1. Radio mosaic at 610 MHz of the F02 field with a resolution of 6 arcsec. Contours are in units of signal-to-noise ratio, and the first contour is 5 times the local r.m.s. The average r.m.s. on the whole image is $50\mu\text{Jy}/\text{beam}$.

that covers the whole image (see Bertin & Arnouts 1996 for more details). To be fully consistent with the analysis of the 1.4 GHz data we adopted the same mesh size, 20 pixels, corresponding to 30 arcsec. Figure 2 shows a contour plot of the noise image. The noise is reasonably uniform in the inner 40×40 arcmin and starts increasing closer to the image borders. The pixel value distribution has a peak at about $50\mu\text{Jy}/\text{beam}$, well in agreement with the average noise value reported in the previous section.

3.2. The source detections

We selected the 1 square degree region centered on the F02 field and within this region we extracted all the radio components with a peak flux $S_P > 150\mu\text{Jy}/\text{beam}$ ($\sim 3\sigma$), using the AIPS task SAD. For each selected component, the peak brightness and total flux density, the position, and the size are estimated using a Gaussian fit. However, for faint components the Gaussian fit may be unreliable and a better estimate of the peak flux S_P (very important since it is used for the selection) and of the component position is obtained with a non-parametric interpolation of the pixel values around the fitted position. Therefore, for all the components found by SAD, we derived the peak flux S_P and the position using a second-degree interpolation fit with the task MAXFIT. Only the components with a signal-to-noise ratio (derived as the ratio between the MAXFIT peak flux and the local noise from the noise map) greater than or

equal to 5 have been included in the sample. Around the brightest sources ($> 10\text{mJy}/\text{beam}$), residual sidelobes can be mistakenly identified with real components by SAD. For this reason we visually inspected the region around bright sources to remove sidelobe spikes.

In this way, we selected a sample of 557 components above the local 5σ threshold. All the components have flux densities greater than 0.2mJy at 610 MHz. The 557 components correspond to 514 sources, since 17 sources are considered as multiple, i.e., fitted with at least two separate components, following the same criteria adopted for the 1.4 GHz catalogue. All the 17 multiple sources at 610 MHz were also found to be multiple at 1.4 GHz.

3.3. Resolved and unresolved sources

To discriminate between resolved and unresolved sources we used the ratio between total and peak flux density. In Fig. 3 we plot the ratio between the total S_T and the peak S_P flux density as a function of the peak flux for all the radio sources in the catalogue. To select the resolved sources, we have determined the lower envelope of the flux ratio distribution of Fig. 3 and, assuming that values of S_T/S_P smaller than 1 are purely due to statistical errors, we have mirrored it above the $S_T/S_P=1$ value (upper envelope in Fig. 3). We have considered extended the 116 sources lying

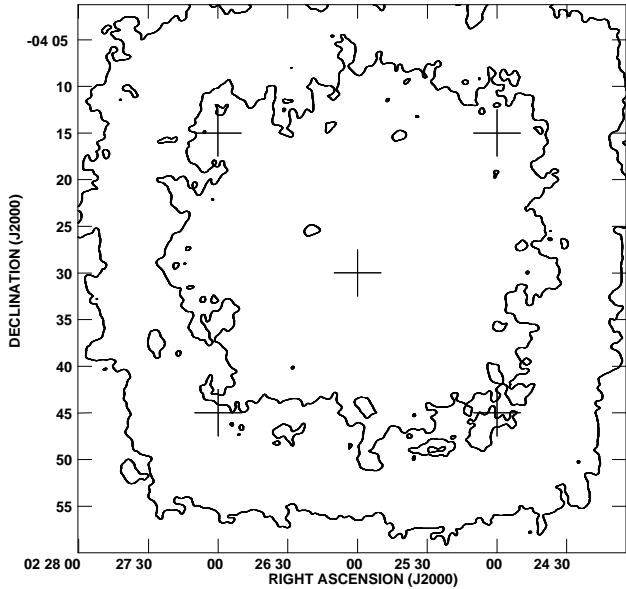


Fig. 2. A contour plot of the noise map obtained with SExtractor. The inner contour contains the region of the image with noise less than $50 \mu\text{Jy}/\text{beam}$, the outer contour the region with noise less than $70 \mu\text{Jy}/\text{beam}$. Crosses show the centers of 5 individual pointings.

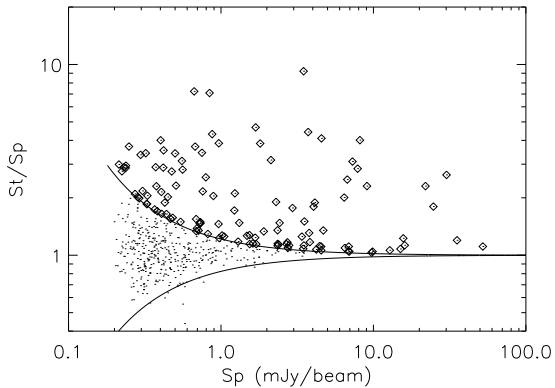


Fig. 3. Ratio of the total flux S_T to the peak flux S_P as a function of S_P . The solid lines show the upper and lower envelopes of the flux ratio distribution containing the sources considered unresolved (see text). Open symbols show the sources considered extended.

above the upper envelope that can be characterized by the equation:

$$\frac{S_T}{S_P} = 0.85^{-(1.2/S_P)}. \quad (1)$$

4. The source counts at 610 MHz

The catalogue is listed in Table 1, available in electronic form at the CDS (<http://cdsweb.u-strasbg.fr/cgi-bin/qcat?J/A+A/>) or through the VVDS radio web page (<http://virnos.bo.astro.it/radio/catalogue.html>). For each entry we list the source name, position in RA and

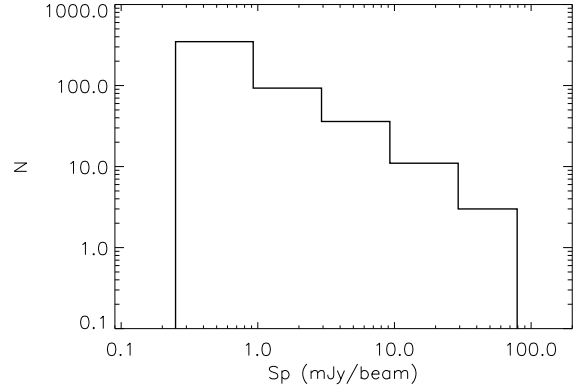


Fig. 4. Peak flux density distribution for all the 514 radio sources at 610 MHz

DEC with errors, peak brightness and total flux density with errors, major and minor axis, and position angle (measured from N through E). The errors were calculated as in Paper I following the relations given by Condon (1997).

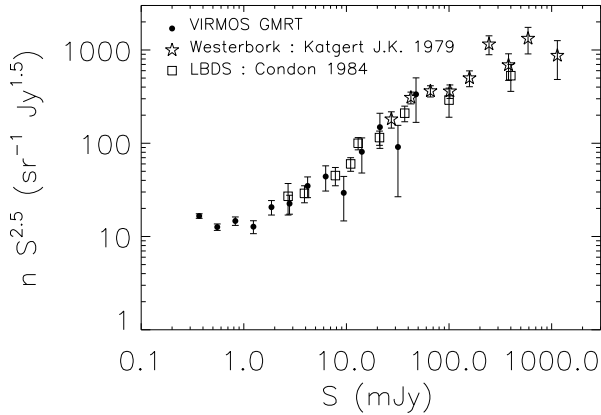
For the unresolved sources the total flux density is set equal to the peak brightness found by MAXFIT and the angular size is undetermined. For each of the 17 sources fitted with multiple components in the catalogue we list an entry for each of the components, identified with a trailing letter (A, B, C, ...) in the source name, and an entry for the whole source, identified with a trailing T in the source name. In these cases the total flux was calculated using the task TVSTAT, which allows for the integration of the map values over irregular areas, and the sizes are the largest angular sizes. The peak flux density distribution of the 514 radio sources is shown in Fig. 4. The catalogue contains 381 radio sources with a flux density less than 1 mJy at 610 MHz (corresponding to 74% of the whole sample) and, to our knowledge, it is the deepest survey at low frequencies ($\nu < 1.4 \text{ GHz}$) obtained so far.

To minimize incompleteness effects in the lowest flux density bin we derived the radio counts using the radio sources with flux density greater than 0.3 mJy. The source counts are summarised in Table 2. For each flux density bin we report the average flux density, the observed number of sources, the number of sources corrected for the visibility area, the differential source density (in $\text{sr}^{-1} \text{Jy}^{-1}$), the normalised differential counts $nS^{2.5}$ (in $\text{sr}^{-1} \text{Jy}^{1.5}$) with estimated Poissonian errors (as $n^{1/2}S^{2.5}$), the cumulative number of sources, and the resolution bias correction. The resolution bias correction accounts for the fact that extended objects with peak flux densities below the survey limit, but total integrated flux densities above this limit, would not be detected by the search procedure. Given a flux density, there will be a maximum detectable angular size beyond which a source will no longer be detectable because its peak flux density drops below the catalogue threshold. To estimate the correction factors to be applied we modeled a population of radio sources extracted from source counts with the integral size distribution derived in Paper I and described by a broken power law consistent with that observed.

The normalized differential counts are shown in Fig. 5 together with other measurements obtained at the same

Table 2. The 610 MHz radio source counts

S (mJy)	$\langle S \rangle$ (mJy)	N_S	N_S^{corr}	dN/dS $\text{sr}^{-1} \text{Jy}^{-1}$	$nS^{2.5}$ $\text{sr}^{-1} \text{Jy}^{1.5}$	$N(> S)$ deg^{-2}	C_{res}
0.30 – 0.45	0.37	145	195.4	4.28×10^9	11.06 ± 0.93	488	1.5
0.45 – 0.68	0.55	93	93.4	1.36×10^9	9.72 ± 1.01	292	1.3
0.68 – 1.01	0.83	64	64.0	6.23×10^8	12.23 ± 1.53	199	1.2
1.01 – 1.52	1.24	33	33.0	2.14×10^8	11.59 ± 2.02	135	1.1
1.52 – 2.28	1.86	32	32.0	1.38×10^8	20.64 ± 3.65	102	1.0
2.28 – 3.42	2.79	19	19.0	5.48×10^7	22.52 ± 5.17	70	1.0
3.42 – 5.13	4.19	16	16.0	3.07×10^7	34.84 ± 8.71	51	1.0
5.13 – 7.69	6.28	11	11.0	1.41×10^7	44.00 ± 13.27	35	1.0
7.69 – 11.53	9.42	4	4.0	3.42×10^6	29.39 ± 14.70	24	1.0
11.53 – 17.30	14.13	6	6.0	3.42×10^6	80.99 ± 33.07	20	1.0
17.30 – 25.95	21.19	6	6.0	2.28×10^6	148.80 ± 60.75	14	1.0
25.95 – 38.92	31.78	2	2.0	5.06×10^5	91.12 ± 64.43	8	1.0
38.92 – 58.39	47.67	4	4.0	6.75×10^5	334.79 ± 167.40	6	1.0
58.39 – 87.59	71.51	1	1.0	1.13×10^5	153.76 ± 153.76	2	1.0
87.59 – 131.37	107.26	0	0.0	0.00	0.00	1	1.0
131.37 – 197.05	160.89	1	1.0	5.00×10^4	518.95 ± 518.95	1	1.0

**Fig. 5.** The normalized differential source counts at 610 MHz. Our results (dots) are shown together with those from 2 other surveys (Katgert 1979; Condon 1984).

frequency from different surveys. Even if not comparable to the deepness of radio surveys at higher frequencies, the source counts obtained for the F02 field at 610 MHz are about one order of magnitude deeper than any previous survey below 1 GHz. Figure 5 clearly shows a flattening of the radio counts around 1 mJy at 610 MHz.

4.1. Comparison with the 1.4 GHz radio source catalogue

Both the 610 MHz and 1.4 GHz catalogues have been derived with the same procedure from images with the same resolution but different sensitivity (the r.m.s. in the 1.4 GHz mosaic is $\simeq 17 \mu\text{Jy}$). The 610 MHz catalogue contains 514 radio sources with flux density greater than $200 \mu\text{Jy}$ compared with the 1054 radio sources with flux density greater than $71 \mu\text{Jy}$ in the 1.4 GHz catalogue. We used all the unresolved sources with flux greater than 0.5 mJy at 610 MHz to derive the systematic offset in right ascension and declination between the two catalogues. Assuming the 1.4 GHz VLA catalogue as a reference, we find a mean offset of $\Delta\text{RA} = -0.14 \pm 0.37$ and $\Delta\text{DEC} = 0.87 \pm 0.40$ arcsec. These

offsets are a fraction of the pixel size and they are expected since the the data sets were self-calibrated. Taking into account these systematic offsets we cross-correlated the two 5σ catalogues using a search radius of 3 arcsec (2 pixels). We found that 448 sources (87%) in the 610 MHz catalogue have a matched counterpart at 1.4 GHz with only 66 sources detected at 610 MHz without a counterpart above 5σ at 1.4 GHz. Given the different sensitivity of the two surveys and the frequency range considered, these 66 sources will have spectral index steeper than ~ -1 . We will return to these sources later in Sect. 6.

5. The spectral index properties of sub-mJy radio sources

5.1. The spectral index catalogue

Both the 610 MHz and 1.4 GHz surveys have the same angular resolution and the catalogues have been assembled using identical procedures. These features are important to derive reliable spectral indices. Moreover, the large number of sub-mJy sources found in these surveys allows us to study the spectral index properties of this class of sources with robust statistics.

The present analysis assumes that the radio sources have not varied significantly in the 4 year interval between the 1.4 GHz and 610 MHz observations. For the general properties of the sample this is a reasonable assumption since a significant variability occurs in only about 5% of the mJy and sub-mJy radio source population (Oort & Windhorst 1985; Windhorst et al. 1985). To study the spectral index distribution of sub-mJy radio sources we started from the 1.4 GHz 5σ catalogue searching for counterparts at 610 MHz within a radius of 3 arcseconds from the position of the component at 1.4 GHz and to a limit of 3σ at 610 MHz. Of the 1054 radio sources in the 1.4 GHz catalogue, 448 are coincident with radio sources above 5σ at 610 MHz, 293 correspond to sources in the range $3\text{--}5\sigma$ at 610 MHz, and 313 have no counterpart above 3σ at the lower frequency. The spectral index catalogue is available as an ascii table at the following address: <http://virmos.bo.astro.it/radio/catalogue.html>. Spectral indices (defined as $S \propto \nu^\alpha$) for the 741 matched

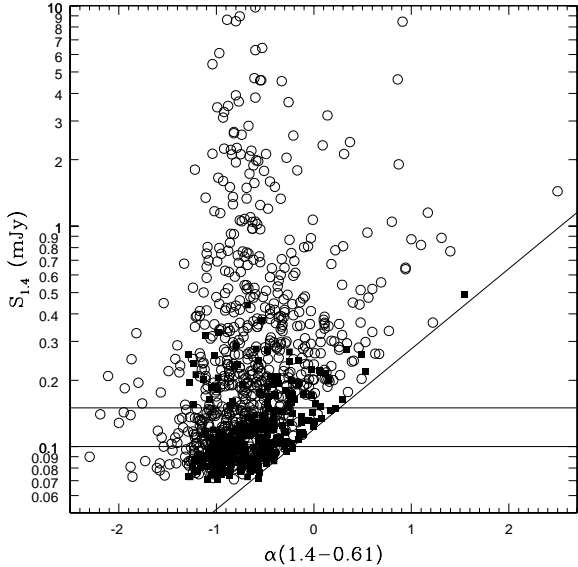


Fig. 6. Flux density at 1.4 GHz as a function of the spectral index between 1.4 GHz and 610 MHz. Filled squares represent lower limits in the spectral index. The solid lines, drawn at 0.10 and 0.15 mJy, are used to illustrate the bias against flat spectrum radio sources at lower flux levels. The slanted solid line shows the maximum value of the spectral index above which no 610 MHz detection is possible due to the flux limit of the 610 MHz survey.

radio sources (with counterparts above 3σ at 610 MHz) are calculated using the total radio flux density at each frequency. Lower limits are derived for the 313 sources without a counterpart at 610 MHz using the peak brightness of the 1.4 GHz component and 3 times the local rms in the 610 MHz image.

5.2. Spectral index versus radio flux density

In Fig. 6 the 1.4 GHz flux density versus the radio spectral index is shown for the 1054 sources (detection and limits). Filled squares are used to indicate the lower limits in the spectral index. Figure 6 clearly shows the well known bias in spectral index due to the different sensitivities of the observations at the two frequencies. In our case, there is a bias against flat spectrum sources at lower flux densities because of the higher flux limit of the 610 MHz observations. For illustrative purposes, we drew two lines corresponding to $S(1.4 \text{ GHz}) = 0.10 \text{ mJy}$ and $S(1.4 \text{ GHz}) = 0.15 \text{ mJy}$. Below 0.1 mJy only the sources with the steepest spectral index can be detected at 610 MHz, and the lower limits dominate (108 detections and 134 lower limits for sources with $S(1.4 \text{ GHz}) < 0.10 \text{ mJy}$). Therefore to avoid such a strong bias, in the following statistical analysis we have considered only the 812 spectral indices (633 detections and 179 lower limits) derived from sources with $S(1.4 \text{ GHz}) \geq 0.10 \text{ mJy}$.

In our analysis we included both the measured values and the lower limits to α_r . The sources were divided into three flux density bins: $0.10 \leq S(1.4 \text{ GHz}) < 0.15 \text{ mJy}$, $0.15 \leq S(1.4 \text{ GHz}) < 0.50 \text{ mJy}$, and $S(1.4 \text{ GHz}) \geq 0.50 \text{ mJy}$, and for each bin we calculated the median value of the spectral index taking into account the lower limits. The statistical difference of the median in the three

Table 3. The radio spectral index versus 1.4 GHz flux

1.4 GHz Flux interval (mJy)	# of detections	# of limits	Median α_{r_med}
$0.10 \leq S < 0.15$	171	110	-0.61 ± 0.04
$0.15 \leq S < 0.50$	304	69	-0.46 ± 0.03
$S \geq 0.50$	158	0	-0.67 ± 0.05

flux density intervals was tested using the software package ASURV, which implements the methods described by Feigelson & Nelson (1985) and Isobe et al. (1986) to properly handle censored data. The radio spectral index of the first and third bin are consistent with being drawn from the same distribution, while the sources with $0.15 \leq S(1.4 \text{ GHz}) < 0.50 \text{ mJy}$ have 99% of probability of being drawn from a different population with flatter spectral index. This result, based on a much larger number of sources than previous works is statistically significant and deserves some comments.

The well known flattening of the normalized source counts appears at $S(1.4 \text{ GHz}) \lesssim 0.5 \text{ mJy}$, so we can expect that the highest flux bin is dominated by classical radio loud AGNs with spectral index ~ -0.7 , consistent with that found. The situation becomes more interesting at lower flux densities where, as we already know from the radio counts, there is a rapid increase in the number of radio sources that is generally ascribed to starburst galaxies, low luminosity AGNs, and radio quiet QSOs. Indeed, we detect a significantly flatter spectral index for sources with $0.15 \leq S(1.4 \text{ GHz}) < 0.50 \text{ mJy}$, meaning that the new population of radio sources emerging below 0.5 mJy has a relevant contribution from flat spectrum compact radio cores that could be hosted in low luminosity AGNs or in radio quiet QSOs. On the contrary, the starburst population is expected to have $\alpha \sim -0.7$ or steeper, since the contribution of thermal radio emission at these frequencies is negligible. It is worth noting that, because of the spectral index bias, we eventually miss radio sources with flat or inverted spectra. Therefore, we can conclude that the flatter radio spectrum of the sources in the intermediate flux density bin compared to those at higher flux densities is statistically significant. Even if it can be difficult to compare results obtained by samples selected at different frequencies, this result is also consistent with that found by Ciliegi et al. (2003) in the Lockman Hole Survey, where radio sources with flux density at 4.9 GHz in the range $0.1 \leq S < 0.2 \text{ mJy}$ have $\alpha_{r_med} = -0.37 \pm 0.10$ compared to $\alpha_{r_med} = -0.81 \pm 0.14$ for the sources at higher flux density.

The interpretation of the spectral index distribution in the fainter flux density bin ($0.10 \leq S(1.4 \text{ GHz}) < 0.15 \text{ mJy}$) is more uncertain due to the increasing weight of the bias against flat spectrum sources. The value of $\alpha_{r_med} = -0.61 \pm 0.04$ mJy suggests that the contribution from flatter spectrum radio cores is decreasing and steeper spectra sources are taking over again. Indeed, evolutionary models of the sub-mJy population predict that starburst galaxies become dominant at $S \lesssim 0.2 \text{ mJy}$ at 1.4 GHz (e.g., Hopkins et al. 1998; Seymour et al. 2004), and the spectral index properties of sources below 0.15 mJy might just be the signature of this effect. Unfortunately, the large number of lower limits in the first flux density bin ($\simeq 40\%$) and the selection effect against sources with spectral index flatter

Table 4. The radio spectral index versus optical type

Optical classif.	# of detections	% of flat spectrum	# of limits	Median α_{r_med}
Early	225	34%	65	-0.55 ± 0.04
Late	80	21%	21	-0.70 ± 0.04
Starburst	37	11%	8	-0.69 ± 0.10
Unidentified	263	34%	64	-0.59 ± 0.04

than $\simeq 0$ that is still present in the first flux density bin make it difficult to draw any strong conclusion.

In summary, the spectral index distribution shows statistically significant differences above and below 0.5 mJy at 1.4 GHz, confirming that a change in the population of radio sources occurs below 0.5 mJy. Radio sources between 0.5 mJy and 0.15 mJy have on average a flatter spectral index, and we interpret this result as being due to the contribution of flat spectrum cores in low luminosity AGNs and radio quiet QSOs. At the faintest flux density level of our survey, the spectral index steepens again, as expected if starburst galaxies become the dominant population, but possible incompleteness effects and the large number of limits makes the statistical significance of this result less secure.

5.3. Spectral index versus optical type

Optical identifications of the 1.4 GHz catalogue were presented in Paper II. On the basis of a maximum likelihood technique, 718 of the 1054 radio sources were identified with optical counterparts and classified in different optical types based on a color-color plot. We adopted a revised classification of the optical type of the identified radio sources based on the best-fit SED template used to estimate the photometric redshift (details on the template sets used to fit the photometric data can be found in Ilbert et al. 2006). Due to the uncertainties of the process, we decided to use only 3 main morphological categories (early-type, late-type, and starburst) and considered only objects whose photometric redshifts are in range $0.2 \leq z \leq 1.5$, where there is an excellent agreement between photometric and spectroscopic redshifts in the VIMOS-VLT deep survey (Ilbert et al. 2006). The results of the spectral index distribution for different optical types are shown in Table 4.

A statistical analysis of the spectral index distribution for each optical classification was performed with ASURV. The median spectral index of the early-type galaxies is significantly flatter than that of late-type objects. Based on all the test of the ASURV analysis, there is a 98% probability that the two distributions are different. Early-type and starburst galaxies have also different α_{r_med} with a slightly less significance because of the larger uncertainty. The unidentified objects have a spectral index distribution indistinguishable from early-type galaxies and with a probability of 95% of being different from that of late-type objects. Finally, the fraction of flat spectrum radio sources ($\alpha > -0.5$) is the same in early-type and unidentified objects, while it is significantly lower in late-type and starburst ones. These results confirm that late-type and starburst galaxies have steeper radio spectra than radio sources identified with early-type objects. The radio spectral properties of the unidentified radio sources suggest that a large fraction of optically unidentified objects is associated with weak (distant or obscured) early-type galaxies.

6. Steep spectrum radio sources and high-redshift radio galaxies

While it is observationally well known that high-redshift radio galaxies (HzRGs) have the steepest spectral indices (usually measured between a few hundred MHz and 1.4 GHz), the reasons why this happens are not entirely understood. Several explanations have been invoked in the literature to interpret this so-called z - α correlation. Most of them assume that the spectral energy distribution of high and low redshift radio galaxies are intrinsically identical and that k -correction and enhanced inverse Compton steepen the spectra of HzRGs (De Breuck et al. 2000, 2002; Pedani 2003; Cohen et al. 2004; Jarvis et al. 2004). Recently, the possibility that HzRGs could have intrinsically steeper spectral indices as they might expand in denser environments has been suggested to explain the radio SED in the SUMSS-NVSS sample of ultra-steep spectrum sources (Klamer et al. 2006).

We used our dual frequency observations of the F02 field to derive a sample of ultra-steep spectrum (USS) radio sources selecting all the radio sources with $\alpha \leq -1.3$. To minimize the inclusion of spurious sources (e.g., noise spikes), we considered only those sources with a $\geq 5\sigma$ detection at one frequency and at least a $\geq 3\sigma$ detection at the other frequency. Finally, to avoid the contribution of steep spectrum nearby sources we excluded all the sources found resolved in the 1.4 GHz catalogue.

The sample contains 39 objects from the 1.4 GHz based spectral index catalogue (i.e. with a $\geq 5\sigma$ detection at 1.4 GHz, and $\geq 3\sigma$ counterpart at 610 MHz). To this sample we added the 19 sources from the complete 610 MHz sample ($\geq 5\sigma$) for which there is a counterpart between 3 and 5 σ at 1.4 GHz. This sample is listed in Table 6, with the name from the 1.4 GHz catalogue, or from the 610 MHz catalogue for those objects with 1.4 GHz flux between 3 and 5 σ , total flux at 1.4 GHz, peak brightness and total flux at 610 MHz, relative errors, and the spectral index.

These 58 sources must be considered as candidate USS sources as several effects can be responsible for the steep spectral index regardless of the intrinsic shape of the radio spectrum. Since the 1.4 GHz and 610 MHz observations are separated by 4 years, radio flux density variability may contaminate the sample. Furthermore, all the 58 USS candidates are weak radio sources: the brightest one is 0.33 mJy at 1.4 GHz. This means that errors in the total flux density determination can also be relatively large, yielding to a less secure spectral index value. Finally, larger fitted sizes for some components at 610 MHz compared to the sizes derived at 1.4 GHz can produce very steep spectral indices. This last effect is certainly affecting some of the sources with the most extreme spectral index ($\alpha < -1.9$) which are fitted with extended Gaussian components at 610 MHz. Anyway, it must be noted that for these sources even considering the peak flux density at 610 MHz instead of the total flux density yields to sources with steep spectral index ($\alpha \lesssim -1$).

Considering all these effects and possible contaminations, the sample of 58 candidate USS sources is still a good starting point to select real ultra-steep spectrum objects and simultaneous multifrequency observations are needed to provide a reliable classification. In particular, it is interesting to note how these candidates are about one to two orders of magnitude fainter than USS sources selected

Table 5. The radio spectral index versus optical magnitude

I_{AB} mag	# of detections	# of limits	Median α_{r_med}
$I_{AB} < 22$	351	80	-0.57 ± 0.03
$I_{AB} \geq 22$	193	33	-0.68 ± 0.04

from previous studies (e.g., De Breuck et al. 2000, 2004) so they could be associated with the most distant USS sources or could be the low radio luminosity counterparts of the HzRGs presently known.

Among the 58 USS candidates 45 are optically identified and we tried to confirm the nature of possible HzRGs using the available optical information. In Fig. 7 we plotted the I_{AB} magnitude and spectral index for all the sources using the following notation: empty circles are sources in the spectral index catalogue and not USS candidates, triangles are sources in the spectral index catalogue and not USS candidates with a lower limit in the spectral index, filled squares are USS candidates that also belong to the spectral index catalogue, and finally empty squares are used to identify USS candidates that do not belong to the spectral index catalogue (sources with 1.4 counterparts between 3 and 5 σ). The small number of USS candidates makes a statistical comparison rather uncertain, but the median of the I_{AB} magnitude for the USS candidates is 21.8 compared to 20.9 for the rest of the sample. What can be appreciated from Fig. 7 is a general steepening of the spectral index going to fainter magnitudes. We have divided all the identified radio sources into two bins of optical I_{AB} magnitude, smaller or greater than $I_{AB} = 22$, and the results are shown in Table 5. The two distributions are different with a confidence level of 99%.

A limited area (625 arcmin²) of the F02 field was observed in the near-infrared K-band optical (Iovino et al. 2005; Temporin et al. 2007). Twelve of the 58 USS candidates fall in this area; 11 out of 12 have an optical/near-infrared identification and 8 out of 11 (73%) have $K_{Vega} > 20$. For comparison, 120 sources from the spectral index catalogue and not USS are identified in the same area and only 65 out of 120 (54%) have $K_{Vega} > 20$. Clearly the statistics are still very limited, but this is another indication of a larger fraction of possible HzRGs in the USS sources compared to the rest of the sample. An estimate of photometric redshifts through the best-fit to the optical/near-infrared spectral energy distribution, following the method described in Ilbert et al. (2006), indicates that these 11 sources are in the redshift range $\sim 0.2 - 3.5$, with only 3 of them having photometric redshift < 1 . The observed spectral energy distributions of these sources are consistent with a variety of spectral types, ranging from elliptical to irregular/starburst. A closer look at their optical and K-band images reveals a high incidence of objects with peculiarities, while the position of the sources in the BzK diagram introduced by Daddi et al. (2004) are consistent with 3 of these sources being $z > 1.4$ star-forming galaxies and 1 a $z > 1.4$ passive galaxy, which also has R–K and I–K colors typical of extremely red objects.

7. Conclusions

We observed the VVDS-VLA field (F02) with the Giant Meter-Wave Radio Telescope at 610 MHz, imaging the 1

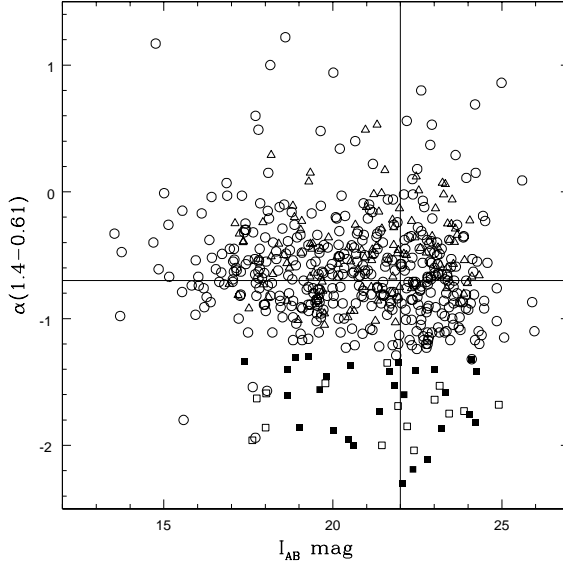


Fig. 7. Two point radio spectral index as a function of the optical I_{AB} magnitude. Dots are used for sources in the spectral index catalogue and not USS, triangles are for lower limits in the spectral index catalogue and not USS, filled squares are USS candidates in the catalogue and empty squares are USS candidates not in the catalogue (with 1.4 GHz counterpart between 3 and 5 σ).

square degree area with an angular resolution of 6 arcsec and an average sensitivity of about 50 μ Jy/beam. A complete catalogue of 514 radio sources down to a local 5σ limit has been compiled and the radio source counts at 610 MHz have been derived. The source counts are the deepest obtained so far at this frequency and clearly show the flattening of the radio counts at about 1 mJy.

The same field was previously observed with the VLA at 1.4 GHz with the same angular resolution. We searched for 610 MHz counterparts of the 1054 radio sources above 5σ in the 1.4 GHz catalogue, obtaining a spectral index catalogue containing 741 matches (448 above 5σ and 293 in the range 3–5 σ at 610 MHz) and 313 lower limits (below 3σ at 610 MHz). Examining the spectral index properties of this catalogue as a function of the radio flux density at 1.4 GHz and of the optical identification we found the following results:

- Above 0.5 mJy the median spectral index is steep ($\alpha = -0.67 \pm 0.05$) and is consistent with being associated with a population of classical radio loud AGNs.
- Between 0.15 mJy and 0.50 mJy the median radio spectral index becomes significantly flatter ($\alpha = -0.46 \pm 0.03$). It is intriguing that the change in spectral index occurs at the same flux density corresponding to the flattening of the radio source counts at 1.4 GHz, suggesting that the new population of radio sources has different spectral properties of the classical radio loud AGNs. In particular, the flatter spectral index seems to rule out the starburst galaxies as the dominant population of radio sources in this flux density interval.
- At the faintest end of the flux density distribution (objects between 0.10 and 0.15 mJy), the median spectral index steepens again ($\alpha = -0.61 \pm 0.04$). Unfortunately,

Table 6. Candidate USS sources

Name	1.4 GHz		0.61 GHz				α
	S_T mJy	σ_{S_T} mJy	S_p mJy/b.	σ_{S_p} mJy/b.	S_T mJy	σ_{S_T} mJy	
VIRMOS1.4GHz_J022402-041343	0.249	0.017	0.507	0.079	1.175	0.183	-1.87
VIRMOS1.4GHz_J022406-044556	0.104	0.018	0.332	0.086	0.332	0.086	-1.40
VIRMOS1.4GHz_J022411-042604	0.090	0.018	0.326	0.062	0.606	0.116	-2.30
VIRMOS1.4GHz_J022413-044642	0.327	0.020	1.484	0.076	1.484	0.076	-1.82
VIRMOS1.4GHz_J022414-041204	0.081	0.015	0.386	0.065	0.386	0.065	-1.88
VIRMOS1.4GHz_J022422-042616	0.157	0.016	0.329	0.066	0.675	0.135	-1.76
VIRMOS1.4GHz_J022423-040229	0.128	0.016	0.408	0.073	0.673	0.121	-2.00
VIRMOS1.4GHz_J022428-041511	0.073	0.015	0.342	0.058	0.342	0.058	-1.86
VIRMOS1.4GHz_J022432-041342	0.250	0.016	0.543	0.061	0.813	0.092	-1.42
VIRMOS1.4GHz_J022436-041031	0.139	0.016	0.306	0.061	0.665	0.133	-1.88
VIRMOS1.4GHz_J022436-041709	0.097	0.016	0.288	0.053	0.288	0.053	-1.31
VIRMOS1.4GHz_J022444-044335	0.096	0.017	0.320	0.053	0.320	0.053	-1.45
VIRMOS1.4GHz_J022447-045851	0.133	0.017	0.418	0.073	0.418	0.073	-1.38
VIRMOS1.4GHz_J022451-045700	0.143	0.018	0.439	0.082	0.722	0.135	-1.95
VIRMOS1.4GHz_J022452-040912	0.084	0.015	0.248	0.049	0.248	0.049	-1.30
VIRMOS1.4GHz_J022517-044602	0.084	0.016	0.270	0.051	0.270	0.051	-1.41
VIRMOS1.4GHz_J022550-042141	0.135	0.016	0.414	0.044	0.414	0.044	-1.35
VIRMOS1.4GHz_J022550-044505	0.122	0.019	0.372	0.049	0.372	0.049	-1.34
VIRMOS1.4GHz_J022611-044005	0.078	0.015	0.289	0.045	0.289	0.045	-1.58
VIRMOS1.4GHz_J022621-040834	0.140	0.017	0.377	0.059	0.867	0.136	-2.19
VIRMOS1.4GHz_J022624-044203	0.209	0.017	0.418	0.049	1.204	0.140	-2.11
VIRMOS1.4GHz_J022638-040845	0.090	0.017	0.270	0.058	0.270	0.058	-1.32
VIRMOS1.4GHz_J022642-044205	0.220	0.017	0.758	0.046	0.758	0.046	-1.49
VIRMOS1.4GHz_J022658-041814	0.217	0.016	0.683	0.050	0.683	0.050	-1.38
VIRMOS1.4GHz_J022700-040501	0.233	0.014	0.467	0.066	0.725	0.103	-1.37
VIRMOS1.4GHz_J022709-045117	0.080	0.015	0.305	0.058	0.305	0.058	-1.61
VIRMOS1.4GHz_J022713-041756	0.083	0.016	0.283	0.054	0.283	0.054	-1.48
VIRMOS1.4GHz_J022716-045719	0.086	0.016	0.363	0.083	0.363	0.083	-1.73
VIRMOS1.4GHz_J022724-042502	0.115	0.016	0.366	0.053	0.366	0.053	-1.39
VIRMOS1.4GHz_J022727-045724	0.288	0.016	0.689	0.083	0.921	0.110	-1.40
VIRMOS1.4GHz_J022735-043159	0.155	0.016	0.466	0.057	0.466	0.057	-1.32
VIRMOS1.4GHz_J022735-044628	0.118	0.018	0.447	0.069	0.447	0.069	-1.60
VIRMOS1.4GHz_J022739-040504	0.074	0.013	0.263	0.067	0.263	0.067	-1.53
VIRMOS1.4GHz_J022741-041736	0.084	0.015	0.312	0.063	0.312	0.063	-1.58
VIRMOS1.4GHz_J022743-044721	0.147	0.018	0.437	0.073	0.437	0.073	-1.31
VIRMOS1.4GHz_J022744-040911	0.103	0.014	0.347	0.067	0.347	0.067	-1.46
VIRMOS1.4GHz_J022745-040559	0.110	0.015	0.359	0.070	0.359	0.070	-1.42
VIRMOS1.4GHz_J022755-044520	0.100	0.019	0.360	0.085	0.360	0.085	-1.54
VIRMOS1.4GHz_J022758-045432	0.110	0.020	0.403	0.102	0.403	0.102	-1.56
VIRMOS0.6GHz_J022414-042922	0.062	0.018	0.338	0.067	0.338	0.067	-2.04
VIRMOS0.6GHz_J022421-041713	0.081	0.017	0.313	0.061	0.313	0.061	-1.63
VIRMOS0.6GHz_J022424-044327	0.060	0.015	0.315	0.063	0.315	0.063	-2.00
VIRMOS0.6GHz_J022503-044807	0.072	0.018	0.271	0.048	0.271	0.048	-1.60
VIRMOS0.6GHz_J022512-044720	0.068	0.018	0.292	0.050	0.292	0.050	-1.75
VIRMOS0.6GHz_J022525-043235	0.050	0.015	0.199	0.039	0.199	0.039	-1.66
VIRMOS0.6GHz_J022538-044658	0.056	0.016	0.286	0.050	0.286	0.050	-1.96
VIRMOS0.6GHz_J022539-042548	0.057	0.015	0.203	0.039	0.203	0.039	-1.53
VIRMOS0.6GHz_J022539-044528	0.067	0.017	0.281	0.047	0.281	0.047	-1.73
VIRMOS0.6GHz_J022552-044233	0.068	0.017	0.265	0.045	0.265	0.045	-1.64
VIRMOS0.6GHz_J022556-043522	0.056	0.018	0.235	0.041	0.235	0.041	-1.73
VIRMOS0.6GHz_J022559-044421	0.078	0.020	0.274	0.051	0.274	0.051	-1.51
VIRMOS0.6GHz_J022626-043657	0.069	0.016	0.211	0.041	0.211	0.041	-1.35
VIRMOS0.6GHz_J022635-042049	0.066	0.017	0.266	0.044	0.266	0.044	-1.68
VIRMOS0.6GHz_J022637-041336	0.070	0.018	0.329	0.046	0.329	0.046	-1.86
VIRMOS0.6GHz_J022641-041602	0.073	0.016	0.296	0.046	0.296	0.046	-1.69
VIRMOS0.6GHz_J022646-041156	0.064	0.016	0.295	0.051	0.295	0.051	-1.84
VIRMOS0.6GHz_J022648-042040	0.064	0.016	0.240	0.045	0.240	0.045	-1.59
VIRMOS0.6GHz_J022715-041648	0.061	0.016	0.283	0.053	0.283	0.053	-1.85

incompleteness effects in this flux density interval do not allow us to draw any strong conclusions for these faintest sources. Nevertheless, it is intriguing to suggest that the possible steepening of the spectral below 0.15

mJy might be associated with the population of strong evolving late type and starburst objects.
 – About 70% of the radio sources are identified with optical galaxies divided into three major categories:

early-type, late-type, and starburst. As expected, late-type and starburst galaxies have indistinguishable spectral index distributions with a median spectral index $\alpha \simeq -0.70$, while early-type galaxies have a flatter median spectral index $\alpha = -0.55 \pm 0.04$. The unidentified objects have spectral properties very similar to those of the radio sources identified with early-type galaxies.

Finally we constructed a sample of 58 candidate USS sources that need further observations to be properly identified as real ultra-steep spectrum sources. The most relevant feature of these candidate USS sources is that they are between one and two orders of magnitude fainter than the USS sources used to find HzRGs. Therefore, they could be associated with even more distant HzRGs, or with low luminosity HzRGs. In both cases these sources represent almost unique objects and it will be very important to confirm their nature of being USS sources and possible HzRGs. In the meantime, we show that there is a general trend for these candidate USS sources to have fainter I-band and K-band magnitudes with respect to the rest of the sources.

Acknowledgements. We thank the staff of the GMRT who have made these observations possible. GMRT is run by the National Center for Radio Astrophysics of the Tata Institute of Fundamental Research.

References

- Afonso, J., Mobasher, B., Chan, B., & Cram, L. 2001, ApJ, 559, L101
Afonso, J., Georgakakis, A., Almeida, C. et al. 2005, ApJ, 624, 135
Afonso, J., Mobasher, B., Koekemoer, A. et al. 2006, AJ, 131, 1216
Benn, C.R., Rowan-Robinson, M., McMahon, R. G., Broadhurst, T.J., & Lawrence, A. 1993, MNRAS, 263, 98
Bertin, E. & Arnouts, S. 1996, A&AS, 117, 393
Bondi, M., Ciliegi, P., Zamorani, G., et al. 2003, A&A, 403, 857 (Paper I)
Ciliegi, P., Mc Mahon, R.G., Miley, G., et al. 1999, MNRAS, 302, 222
Ciliegi, P., Zamorani, G., Hasinger, G. et al. 2003, A&A, 398, 901
Ciliegi, P., Zamorani, G., Bondi, M. et al. 2005, A&A, 441, 879 (Paper II)
Cohen, A.S., Röttgering, H., Jarvis, M.J, Kassim, N.E., Lazio, T.J.W. 2004, ApJS, 150, 417
Condon, J.J 1984, ApJ, 287, 461
Condon, J.J. 1997, PASP, 109, 166
Daddi, E., Cimatti, A., Renzini, A. et al. 2004, ApJ, 617, 746
De Breuck, C., van Breugel, W., Röttgering, H., Miley, G. 2000, A&AS, 143, 303
De Breuck, C., Tang, Y., de Bruyn, A.G., Röttgering, H., van Breugel, W., 2002, A&A, 394, 59
De Breuck, C., Hunstead, R.W., Sadler, E.M., Rocca-Volmerange, B., Klamer, I. 2004, MNRAS, 347, 837
Donnelly, R.H., Partridge, R.B., Windhorst, R.A. 1987, ApJ, 321, 94
Feigelson, E.D., Nelson, P.I. 1985, ApJ, 293, 192
Fomalont, E.B., Kellerman, K.I., Cowie, L. et al. 2006, ApJS, in press astro-ph/0607058
Garrett, M.A., Muxlow, T.W.M., Garrington, S. et al. 2001, A&A, 366, L5
Garrett, M.A., Wrobel, J.M., Morganti, R. 2005, ApJ, 619, 105
Georgakakis, A., Mobasher, B., Cram, L. et al. 1999, MNRAS, 306, 708
Georgakakis, A., Hopkins, A.M., Sullivan, M. et al. 2003, MNRAS, 345, 939
Georgakakis, A., Hopkins, A.M., Afonso, J. et al. 2004, MNRAS, 354, 127
Grupponi, C., Zamorani, G., de Ruiter, H.R. et al. 1997, MNRAS, 286, 470
Grupponi, C., Mignoli, M., & Zamorani, G. 1999a, MNRAS, 304, 199
Hammer, F., Crampton, D., Lilly, S.J., Le Fevre, O., & Kenet, T. 1995, MNRAS, 276, 1085
Hopkins, A. M., Mobasher, B., Cram, L.E., & Rowan-Robinson, M. 1998, MNRAS, 296, 839
Hopkins, A. M., Afonso, J., Chan, B. et al. 2003, AJ, 125, 465
Huynh, M.T., Jackson, C.A., Norris, R.P., Prandoni, I. 2005, AJ, 130, 1373
Ilbert, O., Arnouts, S., McCracken, H.J. et al. 2006, A&A, 457, 841
Iovino, A., McCracken, H. J., Garilli, B. et al. 2005, A&A, 442, 423
Isobe, T., Feigelson, E.D. & Nelson, P.I., 1986, ApJ, 306, 490
Jarvis, M.J., Cruz, M.J., Cohen, A.S., Röttgering, H., Kassim, N.E. 2004, MNRAS, 355, 20
Katgert, J.K. 1979, A&A, 73, 107
Klamer, I.J, Ekers, R.D., Bryant, J.J. et al 2006, MNRAS, in press, astro-ph/0606469
Morganti, R., Garrett, M.A., Chapman, S. et al. 2004, A&A, 424, 371
Norris, R.P., Huynh, M.T., Jackson, C.A. et al. 2005, AJ, 130, 1358
Oort, M.J.A., Windhorst, R.A. 1985, A&A, 145, 405
Pedani, M. 2003, New Astron. Rev., 8, 805
Perley, R.A. 1999, ASP Conference Series, "Synthesis Imaging in Radio Astronomy II", Eds. G. B. Taylor, C. L. Carilli, and R. A. Perley, Vol. 180, p.19
Prandoni, I., Gregorini, L., Parma, P., et al. 2001b, A&A, 369, 787
Prandoni, I., Parma, P., Wieringa, M.H. et al. 2006, A&A, in press astro-ph/0607141
Richards, E.A. 2000, ApJ, 533, 611
Richards, E.A., Kellerman, K.I., Fomalont, E.B., et al. 1998, AJ, 116, 1039
Seymour, N., McHardy, I.M., Gunn, K.F. 2004, MNRAS, 352, 131
Temporin, S., Iovino, A., McCracken, H. J. et al. 2007, in preparation
Windhorst, R.A., Miley, G.K., Owen, F.N., Kron, R.G., Koo, D.C. 1985, ApJ, 289, 494
Windhorst, R.A., Fomalont, E.B., Partridge, R.B., & Lowenthal, J.D. 1993, ApJ, 405 498

Online Material

Table 1. 610 MHz 5σ Catalogue: Sample page

Name	RA (J2000)	DEC J(2000)	σ_{RA} "	σ_{DEC} "	S_P mJy/beam	σ_{S_P} mJy/beam	S_T mJy	σ_{S_T} mJy	θ_M "	θ_m "	PA deg
VIRMOS0.6GHz_J022400-041902	02 24 00.24	-04 19 02.5	0.64	0.55	0.475	0.077	0.475	0.077			
VIRMOS0.6GHz_J022400-044950	02 24 00.89	-04 49 50.8	0.53	0.50	0.806	0.090	0.806	0.090			
VIRMOS0.6GHz_J022402-040731	02 24 02.23	-04 07 31.9	0.62	0.62	0.759	0.080	1.641	0.173	12	7	45
VIRMOS0.6GHz_J022402-041342	02 24 02.73	-04 13 42.2	1.05	0.58	0.507	0.079	1.175	0.183	12	7	101
VIRMOS0.6GHz_J022402-042059	02 24 02.08	-04 20 59.6	0.79	0.75	0.348	0.069	0.348	0.069			
VIRMOS0.6GHz_J022402-042155	02 24 02.56	-04 21 55.4	0.50	0.44	0.823	0.070	0.823	0.070			
VIRMOS0.6GHz_J022402-044136	02 24 02.68	-04 41 36.7	0.64	0.91	0.841	0.072	5.961	0.511	22	14	7
VIRMOS0.6GHz_J022403-040931	02 24 03.14	-04 09 31.7	0.65	0.62	0.750	0.073	2.584	0.252	12	11	119
VIRMOS0.6GHz_J022403-041339	02 24 03.80	-04 13 39.5	0.41	0.41	2.352	0.076	2.640	0.086	7	6	73
VIRMOS0.6GHz_J022403-043305	02 24 03.80	-04 33 05.2	0.41	0.41	4.124	0.084	7.790	0.158	9	8	92
VIRMOS0.6GHz_J022404-044811	02 24 04.13	-04 48 11.2	0.64	0.66	0.435	0.080	0.435	0.080			
VIRMOS0.6GHz_J022405-040950	02 24 05.31	-04 09 50.9	0.49	0.44	0.715	0.069	0.715	0.069			
VIRMOS0.6GHz_J022405-042237	02 24 05.83	-04 22 37.4	0.58	0.55	0.341	0.068	0.341	0.068			
VIRMOS0.6GHz_J022406-045544	02 24 06.09	-04 55 44.6	0.72	0.93	0.442	0.087	0.442	0.087			
VIRMOS0.6GHz_J022408-041134	02 24 08.87	-04 11 34.1	0.43	0.43	1.160	0.068	1.160	0.068			
VIRMOS0.6GHz_J022408-042627	02 24 08.36	-04 26 27.8	0.85	0.87	0.379	0.068	0.379	0.068			
VIRMOS0.6GHz_J022409-041702	02 24 09.77	-04 17 02.6	0.45	0.44	0.918	0.067	0.918	0.067			
VIRMOS0.6GHz_J022409-044254	02 24 09.02	-04 42 54.7	0.49	0.53	0.566	0.079	0.566	0.079			
VIRMOS0.6GHz_J022409-044722	02 24 09.94	-04 47 22.1	0.59	0.49	0.579	0.077	0.579	0.077			
VIRMOS0.6GHz_J022410-042147	02 24 10.03	-04 21 47.7	0.46	0.44	0.788	0.064	0.788	0.064			
VIRMOS0.6GHz_J022410-044607A	02 24 09.58	-04 46 06.4	0.40	0.40	8.943	0.089	13.472	0.134	8	7	102
VIRMOS0.6GHz_J022410-044607B	02 24 10.36	-04 46 08.2	0.40	0.40	24.735	0.086	30.740	0.107	7	6	96
VIRMOS0.6GHz_J022410-044607T	02 24 10.13	-04 46 07.5	0.40	0.40	24.735	0.058	44.500	0.104	30	15	
VIRMOS0.6GHz_J022410-045033	02 24 10.22	-04 50 33.5	0.40	0.40	6.859	0.082	7.207	0.086	6	6	0
VIRMOS0.6GHz_J022411-042604	02 24 11.55	-04 26 04.8	0.95	1.17	0.326	0.062	0.606	0.116	13	6	37
VIRMOS0.6GHz_J022412-041042	02 24 12.27	-04 10 42.0	0.43	0.42	1.065	0.064	1.065	0.064			
VIRMOS0.6GHz_J022412-044043	02 24 12.34	-04 40 43.5	0.47	0.52	0.462	0.071	0.462	0.071			
VIRMOS0.6GHz_J022413-042227	02 24 13.63	-04 22 27.6	0.60	0.53	0.551	0.063	0.551	0.063			
VIRMOS0.6GHz_J022413-042732	02 24 13.63	-04 27 32.1	0.49	0.47	0.798	0.063	0.798	0.063			
VIRMOS0.6GHz_J022413-044642	02 24 13.18	-04 46 42.2	0.42	0.42	1.484	0.076	1.484	0.076			
VIRMOS0.6GHz_J022414-041205	02 24 14.24	-04 12 05.7	0.64	0.53	0.386	0.065	0.386	0.065			
VIRMOS0.6GHz_J022414-041237	02 24 14.16	-04 12 37.0	0.64	0.59	0.339	0.066	0.339	0.066			
VIRMOS0.6GHz_J022414-042922	02 24 14.57	-04 29 22.9	0.94	0.52	0.338	0.067	0.338	0.067			
VIRMOS0.6GHz_J022415-043143	02 24 15.98	-04 31 43.8	0.41	0.41	1.640	0.064	1.640	0.064			
VIRMOS0.6GHz_J022416-042056	02 24 16.07	-04 20 56.8	0.50	0.46	0.591	0.060	0.591	0.060			
VIRMOS0.6GHz_J022419-042028	02 24 19.04	-04 20 28.2	0.62	0.55	0.319	0.059	0.319	0.059			